Novel procedure for laboratory scale production of composite functional filaments for additive manufacturing

Á. Díaz-García[a], J. Y. Law[a], A. Cota[b], A. Bellido-Correa[a], J. Ramírez-Rico[a,b], R. Schäfer[c], V. Franco*[a]

[a] Dpto. Física de la Materia Condensada, ICMSE-CSIC, Universidad de Sevilla, P.O. Box 1065. 41080-Sevilla, Spain.

[b] Centro de Investigación, Tecnología e Innovación de la Universidad de Sevilla (CITIUS), Sevilla, Spain.

[c] Leibniz Institute for Solid State and Materials Science (IFW) Dresden, Helmholtzstrasse 20, D-01069 Dresden, Germany, and Institute for Materials Science, TU Dresden, 01062 Dresden, Germany.

* corresponding author: vfranco@us.es

Successful 3D printing by material extrusion of functional parts for new devices requires high quality filaments. Uniform homogeneity and good dispersion of particles embedded in filaments typically requires several cycles of extrusion or well-prepared feedstock by injection molding, industrial kneaders or twin-screw compounding. These methods require specific production devices that are not available in many laboratories non-specialized in polymer research, such as those working on different material science and technology topics that try to connect with additive manufacturing. Therefore, laboratory studies are usually limited to compositions and filler concentrations provided by commercial companies. Here, we present an original laboratory scale methodology to custom-prepare the feedstock for extruding magnetic composite filaments for fused filament fabrication (FFF), which is attainable by a desktop single-screw extruder. It consists in encapsulating the fillers in custom made capsules that are used as feedstock and reach the melting area of the extruder maintaining the same concentration of fillers. Results have shown that our approach can create smooth and continuous composite filaments with good homogeneity and printability with fine level of dimensional control. We further show the good dispersion of the particles in the composite filament using X-Ray Tomography, which enabled a 3D reconstruction of the spacial distribution of the embedded magnetic particles. The major advantage of this new way of preparing the composite feedstock is that it avoids the hassle of multiple extrusion runs and industrial machinery, yet providing uniform filaments of well controlled filler concentration, which is predictable and reproducible. The proposed methodology is suitable for different polymer matrices and applicable to other functional particle types, not just limited to magnetic ones. This opens an avenue for further laboratory scale development of novel functional composite filaments, useful for any community. This democratization of complex filament preparation, including consumers preparing their own desired uniform novel filaments, will facilitate to unify efforts nearing 3D printing of new functional devices.

Keywords: Additive manufacturing; magnetic composites; soft magnetic materials

1 Introduction

Additive manufacturing (AM) of parts with functional properties by design is a current topic of broad interest as it offers fabricating versatile products of complex geometries for various applications. Such accessible processes using functional composites are mostly limited to extrusion-based and photo-solidification methods, where the active particles, such as ceramics [1], metals etc., are added to the printing matrix (e.g. PLA (polylactic acid), ABS (acrylonitrile butadiene styrene), etc.) to make magnetic [2–6] or electrically conductive [7] filaments and thus bring functionality to the final printed composite product. For the latter technique, also known as stereolithography-based printing, using a mixed powder-liquid suspension, wherein the liquid is photo-curable resin, creates green parts with arbitrary final 3D shapes. Its constraints entail (1) limited filler loading that can greatly affect the photocuring of the resin for higher filler content; (2) heterogeneity in the filler distribution within the printed component that can be caused by the instability of the resin-filler suspension [8]. On the other hand, the extrusion-based process builds up the object through layer-by layer deposition of a fused filament. This is also commonly known as fused filament fabrication (FFF) or fused deposition modelling (FDM) and remains the most popular AM technique due to its competitive cost and easy tuning of process parameters for different feedstock types. However, there is still a limited variety of commercial composite filaments though a wide range of composite feedstock materials is commercially available. One should also note that the used fillers, whose compositions are restricted to those provided by industry, might not be the most optimal for 3D printing of functionally active devices with desired performance. Hence, laboratory scale formulation and subsequent production of composite filaments with robust and reproducible high-performance or catered properties remains a challenge, which involves a variability of polymer matrix, the selection of functional fillers with desired properties, and the predictable control of filler loading into the filament.

Recent developments related to print-compatible composite functional materials mostly involve embedment of metallic particles, carbon fibers, carbon nanotubes, etc. in polymer matrix filaments [7,9–11]. However, the commercial filament that can be magnetic is mostly limited to rustable iron-filled PLA filament (11.5 vol.% or 40, 46 wt.% reported in refs. [2,12,13] respectively). This is in contrast with the broad applicability of magnetic materials, including their uses in power generation and transmission, electronic appliances, digital data storage, sensors, actuators, magnetocaloric refrigeration, etc. [14]. New potential applications of this type of composite

polymers can be based on the heating that soft magnetic particles exhibit when an alternate magnetic field is applied. For example, this radio-frequency heating of magnetic particles could be used to cure a polymer or epoxy binding matrix in a functional form for such applications as EMI absorbers [15]. In the case of soft magnetic applications with a large fraction of magnetic materials, such as transformer cores, the reported 3D printing for developing devices so far relied on the use of commercial supply [5,6].

The development of new composites for FFF reported in the literature mainly adopts the following approaches, with some major limitations in parenthesis:

- Chemical method of mixing the filler and polymer matrix → single-screw extrusion (leading to a highly non-homogenous filament) → cut into composite pellets → re-extrude → repeat cutting and re-extrusion (typically 6 extrusion cycles are required to obtain a homogenous composite filament [8], involving a long processing time and a limited predictability of the final concentration);
- Chemical method of mixing the filler and polymer matrix → twin-screw extrusion (produced filament was with limited ovality despite using twin-screw extruder [16]; twin screw extruder not available in most laboratories outside polymer research);
- feedstock pellets prepared by industrial kneaders and/or compounding or simply bought from industrial compounded grades → extrusion [17–20] (reliance on industrial procedures that are not available in small scale laboratories, or limitation to the compositions and concentrations industrially available).

In short, the quality of the functional composite filaments (including the particle distribution within the matrix) is highly dependent on the feedstock for final extrusion, which also, in turn, affects the functional properties of the fabricated parts. Industrial grade kneaded and compounded composite feedstock is the typical and fastest option used for extruding magnetic filaments for 3D printing despite there are challenges in getting a smooth filament and printing with a high filler content [3,21]. These specific machineries are typically inaccessible in most laboratories, which will not be a competitive option for studying AM with diverse functionalities in mind while a good reliable composite filament for printing remains a challenge. For non-reliance on industrial machinery, the extrusion has to be repeated for several multiple runs to develop own feedstock of good quality prior to extruding a homogenous composite filament. These challenges are also highlighted in ref. [22], wherein the authors report non-uniformity of the metallic particle distribution within the composite PLA-Mg filament even for low loading (4 g of fillers was used for

150 g of PLA). In addition, any successful composite print would be challenging when using filaments with inhomogeneous distribution of the functional particles.

Therefore, to be able to extend the research on the printing of functional parts and their performance, a viable laboratory scale procedure for filament production is needed. To be able to eventually improve the performance of the functional parts, researchers need to have control over the customizable characteristics of the magnetic composite filament (e.g. particle filler composition and properties, particle shape, volume percent and dispersion within the polymeric matrix)[6]. Furthermore, it is challenging to extrude composite filaments containing significant amounts of functional or structural particles. This issue has been raised in ref. [8] for the following reasons: (1) homogenous distribution of the filler materials within the filament is a must so as not to compromise the structure and function of the printed component; (2) a suitable flexibility, strength and smooth texture of the developed composite filament together with a consistent diameter is essential to reliably feed it into the extrusion nozzle of a FFF printer for continuous printing; (3) the viscosity (or other related properties) of the melted feedstock, caused by the loading of particles to the base polymer, will be modified and thus should not cause blockage or damage to the nozzles of the extruder or print head. Furthermore, while most of the research on magnetic filaments focused on permanent magnets with high filler content, soft magnetic particles uniformly embedded in the part with a low concentration will allow to develop not only functional parts but “smart parts” that are able to monitor their state while in operation, like temperature (via thermomagnetic properties of the fillers), stress (via magnetoelastic response), etc.. The uniformity of fillers in low concentrations is even more challenging than that of highly loaded filaments.

The main goal of this work is to present a procedure that would advance the possibilities of developing functional composite filament in laboratories with a simple filament extruder, starting from pure polymer and fillers, showing that the functional filament is printable. As a concept validation approach, maraging steel particles as the soft magnetic material filler, PLA (a typical polymeric material for FFF) as the polymer matrix, and the typical printing capabilities of research laboratories are used. This study reports the first proof-of-concept demonstration of preparing customized feedstock for composite filament extrusion without any special machinery or chemical procedure, yet allows a good control of the filler concentration and distribution in magnetic composite filaments using a single-screw extruder. We have characterized the extruded

composite filaments by magnetization measurements as well as advanced microstructural characterization techniques, such as scanning electron microscopy (SEM), X-ray tomography, and magneto-optical Kerr microscopy. The results show a good agreement between the actual compositions of the fabricated magnetic composite filaments with the nominal composition of the feedstock, proving homogeneously distributed magnetic fillers in the composite filament. In addition, a uniform distribution of the particles within the PLA matrix is found for low filler loading of 5 vol.%. Furthermore, the printability of the developed composite filament with the highest prepared content of fillers (12 vol.% maraging steel, which corresponds to 47.5 wt.% , thus being comparable to the literature and commercial magnetic rustable iron composite filaments), is successfully achieved without the need of a thorough optimization of the printing parameters. The proposed technique is not restricted to just magnetic functional material fillers but any other fillers could be used.

2 Experimental techniques

The starting materials to produce the composite filaments were commercial PLA pellets and soft magnetic, gas-atomized maraging steel powders (particle sizes <20 µm). A 3devo NEXT 1.0 ADVANCED extruder was used. It comprises of a single screw extruder (L/D ratio = 15 : 1, pitch distance = 25mm). A printer Ultimaker S5 was used for all the 3D printing tasks performed in this work.

The morphologies of the powder and cross-sections of the fabricated composite filament were examined using a scanning electron microscope (FEI™ Teneo). In addition, the interior features of the composite filament were further quantified using micro-computed X-ray tomography to obtain relevant information on the homogeneity of the PLA-maraging steel filament. This was performed using the Easytom XL 160 system (RX Solutions, France), equipped with an open X-ray (LaB6) tube that produces a spot < 500 nm wide at the tungsten anode for a resolution of < 1 µm. A cylindrically shaped section of ϕ1.8 mm x 1.1 mm from the interior of the filament was used for imaging at a voxel size of 1.00 µm. For additional analysis, a cubic sub-volume of 1.0 mm length was further cropped. Further quantification of the filler content in the composite filament was obtained by using thresholding by the MorpholibJ suite of plugins [23] in FIJI [24,25]. Its volume fraction was determined by the sum of the volumes of the analyzed particles out of the total volume of the composite filament. The particle fillers apparently in contact with each other were separated using the distance transform watershed 3D algorithm calculated upon segmentation by volume

thresholding. The connected volumes were then assigned to individual particles and labelled for further analysis upon excluding those in contact. The volume, surface area and coordinates of the center of mass of each particle were calculated. Particle sphericity was determined as:

$$\text{sphericity} = 36\pi \frac{V^2}{S^3} \quad [1]$$

where *V* and *S* represent volume and surface area of each particle. The effective diameter of the particle, *d*, (assumed as an equivalent sphere) was calculated as:

$$d = \left(\frac{6V}{\pi}\right)^{1/3}, \quad [2]$$

which enables the determination of the particle size distribution of the maraging steel. In addition, the mean separation between each particle and its nearest neighbor was investigated by the 3D-construction of a Delaunay triangulation (using the coordinates of the center of mass of the particles as vertices in MATLAB), wherein the extracted mesh of edge lengths yields the distance between the fillers.

Since the filaments have been intentionally manufactured to exhibit specific soft magnetic behavior, they have been magnetically characterized to show their potential applicability for manufacturing magnetic parts. The magnetization of the starting maraging steel powder and magnetic composite filament were characterized using a Lake Shore Cryotronics 7407 vibrating sample magnetometer (VSM). Hysteresis loops at room temperature were measured to check the soft magnetic behavior of the starting magnetic powder and composite filaments and to get their saturation magnetization as it is essential to know these characteristics for the application of the filaments in functional magnetic pieces. Samples of the filaments were taken every 0.15 m to further evaluate the homogeneity of the composite.

To reinforce the conclusions from the structural characterization and from the magnetization results, Kerr microscopy, that combines both types, has been carried out. By using this technique, the soft magnetic character of particles in the composite filament can be verified after the fabrication of the composite, and details of whether there are interactions between the particles, related with the distribution of the particles in the polymeric matrix, can also be analyzed. The magnetic domains on a selected composite filament were imaged by high-resolution wide-field Kerr microscopy using a 100x oil immersion lens with a numerical aperture of 1.3 [26]. For imaging,

a 1 mm thick disk was cut from the filament and carefully polished with a colloidal Si-suspension (OP-S from Struers) to avoid residual polishing stress on the exposed particle surfaces [27].

3 Filament fabrication methodology

The inhomogeneity of the filler distribution and unpredictable filler content in filaments produced using conventional techniques with desktop filament extruders originate from the retention of the filler particles at different parts of the extruder. Therefore, the main goal of our proposed procedure is to avoid these two problems by preparing capsules, made of the polymeric material, loaded with filler powder. Being the fillers inside the polymer capsules, no powder retention or loss can occur along the way until the melting zone is reached. In addition, as all capsules have been manufactured in the same way, they can contain equal amounts of powder and polymer. This leads to a flow of material through the extruder with a very constant proportion of both components so the polymer is melted and mixed with the functional powder in desired fraction. Mixing of the polymer and powder takes place in the melting and mixing parts of the extruder barrel and the eventual filament consists of uniformly distributed particles in the polymer matrix.

No additional procedure was necessary to get a proper dispersion of this type of soft magnetic particles in the polymer matrix or to avoid particle agglomeration. Through the use of the proposed encapsulation technique the different components reach the melting and mixing zones of the extruder together but not blended. The combined effect of temperature and mechanical action in the melting area of the extruder prevents agglomeration of the particles. A later mixing area in the extruder helps the uniformity of the filament. For the extrapolation of this method to particles that tend to agglomerate, the typical variables that affect the compounding (e.g., polymer material, mixer type, rotor geometry and speed, temperature, etc.) and the need for additives or surface treatment of the fillers should be explored [28], although no significant difficulty is expected beyond the usual optimization requirements for the extrusion.

3.1 Feedstock Preparation

The feedstock for the filament extrusion was prepared with the customized procedure of composite encapsulation as summarized in Figure 1. Initial PLA capsular templates were designed and 3D printed (shown on the left of Figure 1) for the subsequent loading of particle fillers (gray spherical representation). The filling procedure of the capsules was conducted manually, leveling at all times the amount of powder up to the surface of the templates, so that all the capsules are completely filled, providing equal capsules to be used as feedstock. The encapsulation of the powders was subsequently performed by using a PLA lid to cover the powders in the capsular

template and sealing with acetone. Both, the stages of loading as well as encapsulating the powder can be considered critical phases of the procedure as any gap or air sacs will affect the rigidity of the filled composite capsules when cutting the templates or when transporting them into the hopper for extrusion. The sealing of the fully filled capsules with flat covers printed using only two layers minimizes the appearance of air bags with the addition of as little extra polymeric material as possible. In addition, the weights of the PLA capsular templates and cover lids were recorded before loading the powder. The composite capsules (loaded with powder) were then dried at 50˚C in a furnace for 15 min to remove any traces of acetone before recording the weights of the dried and sealed capsules. The difference in the recorded weight data before and after powder loading was then used as the nominal weight fraction of the feedstock. The final step prior to extrusion involves that the template arrays were cut into sealed capsules of similar size and shape.

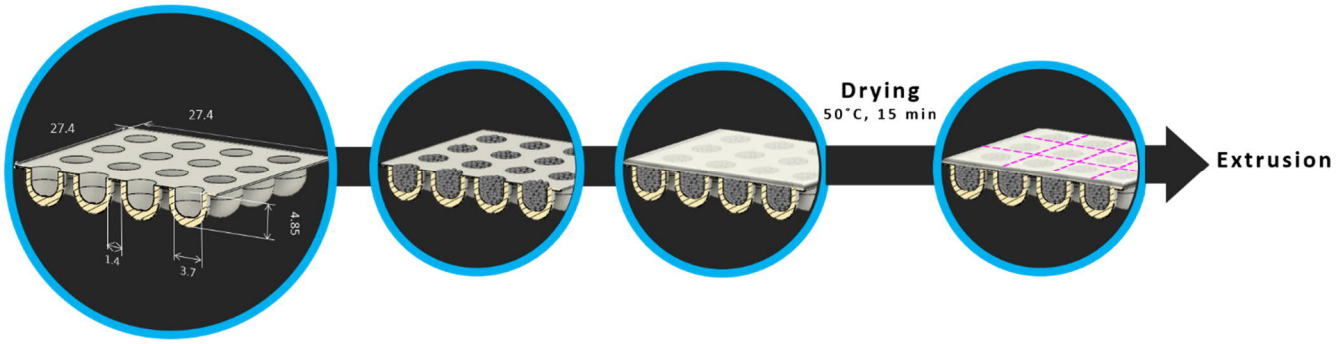

Figure 1. Schematic representation of the methodology approach (starting from far left): PLA capsular template (dimensions are in mm), highly-packed capsules with fillers (maraging steel), encapsulation of the composite pellets as feedstock. These were further dried at 50 ˚C for 10 minutes before cutting them into capsules of similar size and shape (dotted pink lines depict as the cut lines) for subsequent extrusion.

The microencapsulation of fillers by chemical procedures is a known technique for compounding of polymers that is used in cases where, for example, it is necessary to protect the fillers from the environment (e.g. from moisture) or to increase the interaction between the fillers and the polymer matrix [29–31]. The proposed method is different from that both in the methodology and the purpose. Mechanical encapsulation of the fillers to produce a suitable feedstock for extrusion is also found in the literature [32]. The usual procedure is to mix the melted polymer and the filler powders in a kneader, let the mixture solidify and cut it into pellets before extrusion. All these procedures depend on additional equipment beyond the filament extruder and imply several kneading steps before uniform pellets are obtained.

Here we fill macro-capsules with the functional particles to replicate the common polymer pellets that are used for filament extrusion (with a typical size of several millimeters). This simple procedure can be carried out with the most basic instruments of a laboratory that can produce filaments for 3D printing: a desktop 3D-printer and a desktop extruder. Despite its simplicity, the procedure allows that the polymer and functional particles reach the melting and mixing zones of the extruder in the desired fractions without the need of previous kneading or chemical blending of the feedstock.

Nominal filler ratios of the composite, varying from 5 to 12 vol.% maraging steel (corresponding to 25 – 47.5 wt.%), were selected for this study. The custom-made composite capsules were mixed with appropriate an amount of PLA pellets (they are of the same sizes and shapes to ensure appropriate mixing and uniform flow of the extruded material) to tune for the nominal composite ratio as the feedstock. Alternatively, capsular templates with different available volume for filling with powder can be prepared.

It is important to mention that 3D printing of the capsular templates extends the procedure to virtually any polymeric material that can be used in 3D printing (the final goal of the filament), even for those types which are not commercially available as capsules or which are not of the proper size. For those types of polymers with suitably available commercial capsules, it is simpler to directly use them to encapsulate the filler powder, skipping one of the preliminary steps of the proposed procedure while the main methodological procedure remains the same.

3.2 Filament Fabrication

Once the customized feedstock of maraging steel-filled PLA composite pellets was properly prepared, it was loaded into the hopper of the desktop single screw extruder, which incorporates four independent heaters along the mixing zones. For the experiments, the various heaters were set as 170 °C – 185 °C – 190 °C – 180 °C with the rotor at 5 RPM, which are typical parameters for PLA extrusion. The diameter of the filament ($\phi_{\,composite\ filament}$), set at a nominal value of 2.85 mm, was dynamically controlled by in-situ measurements made by an optical sensor that also provided a feedback control to the automated winding system of the extruder. The fabricated composite filaments were typically about 7 m long, which corresponds to a typical value of 400 capsules for the largest volume concentration of powder. The complete run lasted for not more than 2 hours

including the waiting time for the temperature stabilization of the heating zones in the extruder. To speed up the procedure for a more massive production of materials for which capsules are not available, instead of 3D printing the capsules, they can be vacuum formed or thermoformed with simple laboratory-made devices.

4 Characterization of the filaments

4.1 Physical Characteristics

Figure 2 shows the physical examinations of the composite filament. The in-situ measurement of $\phi_{composite\ filament}$ as displayed in Figure 2 (a) shows oscillations around an average value of 2.844 mm (RMS error of 0.109 mm), which agrees reasonably well with the nominal diameter (2.85 mm) as such small fluctuations would not be critical for the use of the filament in a 3D printer. Therefore, the size and the final hemisphere shape of the capsules was not found to be an inconvenience for the flowability of the feedstock in the used extruder. Further studies for the optimization of the capsular shapes is underway. The diameter assessment was further performed on the cooled composite filament, showing an average value that is in good agreement with that previously determined in-situ, indicating no shrinkage. Furthermore, the extruded composite filament (gray in color) is magnetic, which can be observed in Figure 2 (b), wherein it is being supported by a permanent magnet on the whiteboard. A photograph of the cross-section of the filament is presented in Figure 2 (c), showing an overall view of the particles evenly distributed in the PLA matrix instead of confining to the core or edge of the filament.

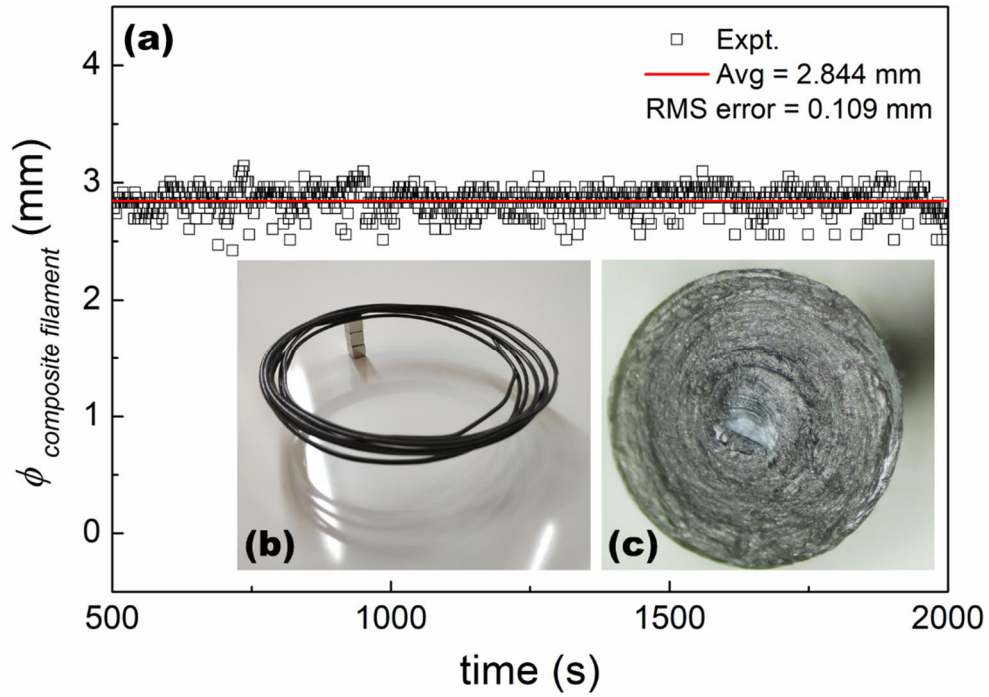

Figure 2. Physical examination: (a) In-situ measurements of the diameter of composite filament during the extrusion; photographs of the (b) magnetic composite filament (attracted to a permanent magnet) and (c) cross-section of a composite filament.

4.2 Morphological characteristics

Figure 3 shows the scanning electron microscopy (SEM) images of the as-received maraging steel powder, the cross-sections of the composite filaments and their backscattered electron (BSE) images. The SEM image of the maraging steel particles in Figure 3 (a) shows that they are of spheroidal shape with a broad size distribution. For the cross-sections of the composite filaments (Figure 3 (b) – (d)), their SEM images show that the particle fillers (i.e. maraging steel) embedded in the PLA matrix maintain their spheroidal shape, indicating that the manufacturing process has not altered the magnetic fillers. A maximum temperature of 190 °C was reached during the filament fabrication process, which is insufficient to affect maraging steel, thus preserving the properties of the fillers. The backscattered electron (BSE) images of the cross-sections of the various composite filaments further show that the particle fillers are distributed throughout the filament.

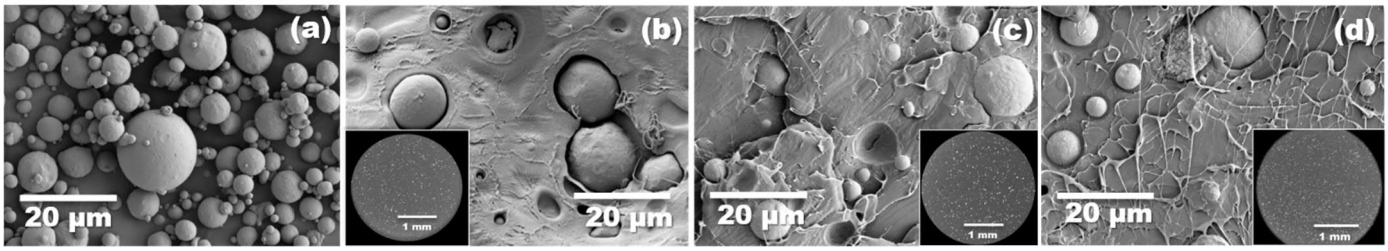

Figure 3. SEM images of (a) maraging steel powder, cross-sections of the composite filament with nominal (b) 5 vol.%, (c) 8 vol.%, and (d) 12 vol. % of fillers. The corresponding BSE images of the composite filaments are also included as insets.

4.3 Interior characteristics of the composite filament via 3D-sectioning from X-ray tomography

Typically for low filler compositions, its limited loading can pose challenges in obtaining evenly distributed particles throughout the useful length of the filament. However, this can be relevant when the embedded sensing particles in the filament are to be printed as “smart parts” to give information about their local operation conditions. Hence, the interior characteristics of the composite filament of nominal 5 vol.% maraging steel were also characterized using X-ray tomography and their results are presented in Figure 4. A lateral slice from the center of the reconstructed volume (with the rotation axis perpendicular to the page) is displayed in Figure 4

(a) and its segmentation results (upon thresholding) in Figure 4 (b). After applying the algorithm for separating the particles in contact (from the same slice in Figure 4 (a) and (b)), the various detected particles are color-labelled (as shown in Figure 4 (c)) to ease identifying the neighboring particles. The sum of the particle volumes was determined, estimating the fraction of particle fillers in the composite filament as 5.5±0.5 vol.%. This is in good agreement with the nominal composition of the composite feedstock. Furthermore, Figure 4 (c) reveals that the particle fillers are evenly distributed inside the volume of the composite filament. Figure 4 (d) shows a section of the Delaunay triangulation, with straight lines connecting each particle to its neighbors. A 3D representation of the particles is displayed in Figure 4 (e) for a smaller cubic volume with 300-µm edges. The particles are assigned to different colors based on their sizes, ranging from 5 – 35 µm as indicated in the legend. Videos including 3D reconstruction of the composite filament are available in the supplementary information.

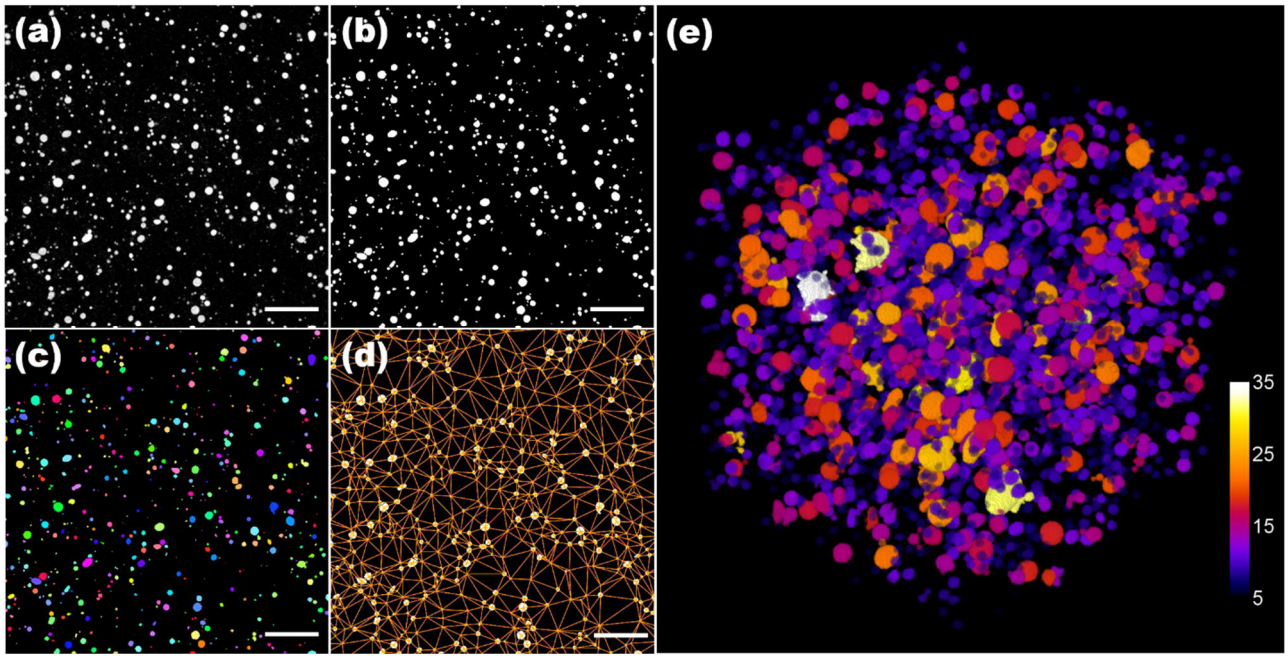

Figure 4. X-ray tomography results of the composite filament with nominal 5 vol.% maraging steel content: (a) slice of the reconstructed volume of the filament, (b) upon thresholding; (c) with particle labeling (randomly assigned colors) with the algorithm application; (d) after Delaunay triangulation for interparticle distance determination. (e) Detected particles from a smaller subvolume labelled by colors corresponding to their particle sizes. Scale bars in panels (a) to (d) represent 100 µm.

The distribution of particle sphericity is further analyzed in a histogram as shown in Figure 5 (a). Most particles are very close to spherical shape, with more than 75% of the particles exhibiting sphericity in the 0.9-1.0 range. The particle size distribution of the composite filament is shown in

Figure 5 (b), wherein the blue bars and green line represent the relative and cumulative frequencies respectively. The relative size distribution was fitted to a log-normal distribution (magenta line) to calculate the average particle size (*P*) and its standard deviation. The log-normal distribution is given by:

$$P(d) \propto \frac{1}{\sqrt{2\pi\sigma^2}}\frac{1}{d}\exp\left[-\frac{(\ln d-\ln \mu)^2}{2\sigma^2}\right], \quad [3]$$

where the fitted parameters are μ and σ. Hence, the mean particle diameter,$\bar{d}$, and variance, σ_d, are calculated according to:

$$\bar{d} = \mu\, exp\left(\frac{\sigma^2}{2}\right). \quad [4]$$

$$\sigma_d = \bar{d}\sqrt{\exp(\sigma^2) - 1} \quad [5]$$

The calculated mean particle diameter based on the X-ray tomography result is $\bar{d}$ = (6 ± 4) µm. The distribution of the inter-particle distance (first neighbors only) can also be determined. It is presented in Figure 5 (c), showing an overall mean separation of 22 ± 10 µm. The fact that the average distance is much larger than the average diameter is an indication of the lack of agglomeration of the particles within the studied volume.

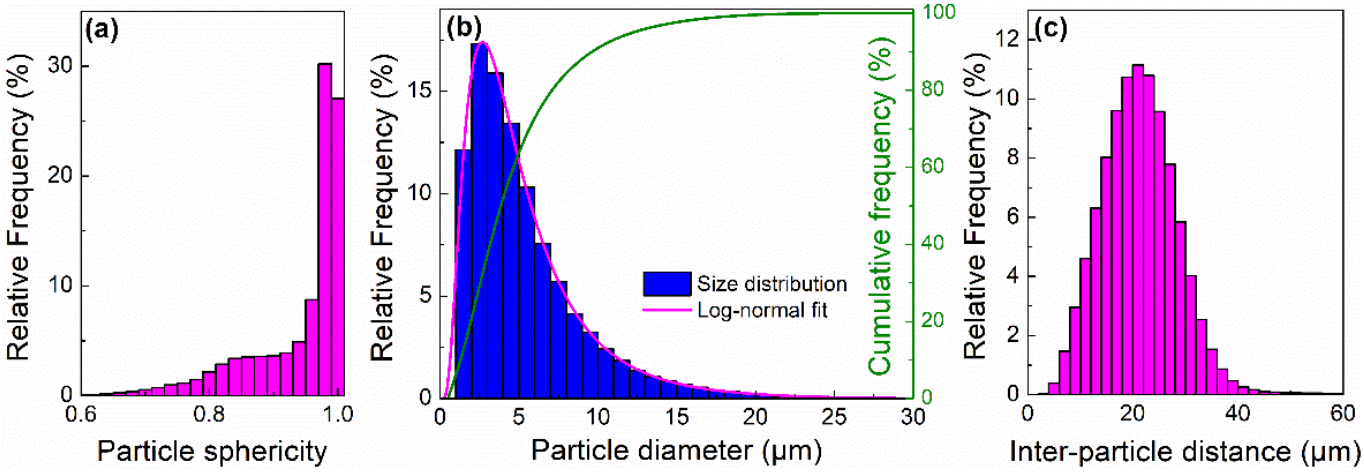

Figure 5. Further calculation analyses from the X-ray tomography data: (a) particle sphericity distribution; (b) particle size distribution, wherein the relative and cumulative frequencies are represented by the blue bars and green line while the fitted log-normal distribution appears as a magenta line; (c) the distribution of inter-particle distance.

4.4 Functional Magnetic Characterization

Figure 6 shows the magnetization (M) of maraging steel powder as a function of magnetic field (H) measured at room temperature, evidencing a very soft magnetic behavior and a saturation magnetization (M_S) of 110.58 A m^2 kg^{-1}. In addition, the $M(H)$ raw data of the composite filaments normalized by the composite mass (labelled by nominal compositions) are included for comparison. The composite filaments show a soft magnetic behavior like the maraging steel powder but with varying saturation magnetization values due to the different amount of magnetic fillers. The saturation magnetization, M_S, is observed to increase with larger nominal fraction of the magnetic fillers in the composite. Hence, the amount of magnetic fillers in the composite filaments was independently determined using the densities of the phases and comparing the M_S of the composite filaments to that of the powder. Results are tabulated in Table 1. The calculated compositions of the composite filaments agree well with the nominal composition of the feedstock for the filament extruder and with the X-ray tomography results shown above. On top of that, it is worth mentioning that the composite filament of nominal 12 vol.% fillers, with the calculated composition of 12.2 vol.% corresponding to 47.5 wt.%, has a composition that lies in the reported range of the commercial magnetic filament (magnetic Fe in PLA reported to exhibit 11.5 vol.% in ref. [12], and 40 and 46 wt.% in ref. [13] respectively). It was fabricated, however, without any reliance on industrial machinery. Furthermore, reported magnetic filaments with such an amount of volume loading, are typically fabricated using industrial feedstock [3,12]. The shape of the $M(H)$ curves of the composite filaments are different from that of the powder (especially the slopes before saturation) due to the different demagnetizing factors.

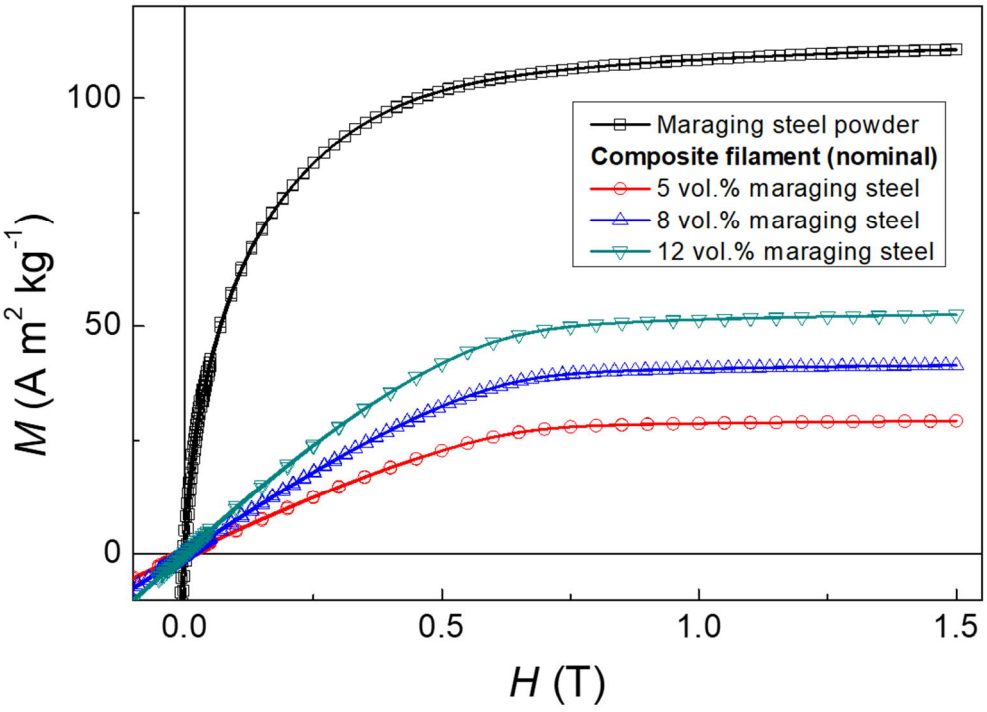

Figure 6. *M*(*H*) raw data of the maraging steel powder and various composite filaments (labelled by their nominal compositions).

Table 1. Fraction of fillers in the composite filaments determined from VSM data.

Sample	M_S (A m^2 kg^{-1})	Amount of magnetic fillers in the composite filament determined from M_S	
		vol. %	wt.%
Maraging steel powder	110	100	100
5 vol.% nominal	29.22	5.3	26.4
8 vol.% nominal	41.40	8.5	37.5
12 vol.% nominal	52.47	12.2	47.5

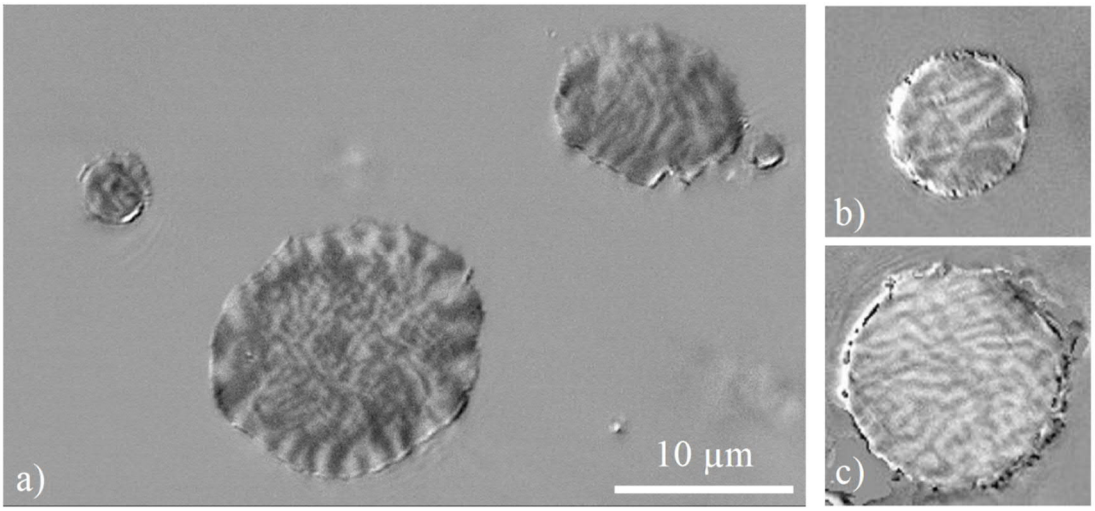

Figure 7. Magnetic domains of cut and polished maraging steel particles (5 vol. %) embedded in the composite filament imaged by Kerr microscopy: in (a) a neighborhood with three particles, while the particles in (b) and (c) appeared isolated.

Figure 7 shows the imaging by Kerr microscopy of nominal 5 vol.% composite filament. Typical magnetic domains and particles with sizes ranging between 4 and 15 µm are observed. The domains were imaged in pure in-plane Kerr sensitivity [33] along the horizontal axis after AC-field demagnetization in (a) and at remanence after switching off a saturating magnetic field along the horizontal in-plane direction in (b, c). For interpretation, the following remarks need to be considered. (i) The shown domains are observed on particles that were cut by polishing. For energy reasons, the domains adapted to the imaged surface are not necessarily representative for the bulk of uncut particles [34]. Nevertheless, domains sizes in a similar range are also expected for the volume, owing to the finite size of the particles. (ii) Under polar contrast conditions with pure Kerr sensitivity to out-of-plane magnetization, no domain contrast was detected (not shown). Consequently, the shown domains are strictly magnetized in-plane, enforced by dominating stray field energy. This is a typical feature of low-anisotropy materials, supporting our former assumption that the individual particles are of soft magnetic character. (iii) For the 5 vol.% sample, no traces of magnetic stray-field interaction between the particles can be concluded from the observed domains, which indicates a good dispersion within the matrix (in agreement with X-ray tomography results). (iv) Domain sizes ranging between sub-micrometers up to several micrometers are found. It is likely that the finer patterns are closure domains of underlying volume domains with some perpendicular component of magnetization in the bulk of the particle. It cannot be further determined whether the variety of domain scales is related to the crystallographic grain structure of the particles or to some induced anisotropy caused by (internal) mechanical stress. Nevertheless, an inhomogeneous distribution of anisotropy seems to be

typical. It is, however, unlikely that this will play a significant role for the magnetization behavior of the whole ensemble of embedded particles, which seems to be dominated by demagnetization effects rather than by anisotropy.

4.5 3D printing

One common issue with highly loaded composite filaments is nozzle clogging or their mechanical inability for printing [3,21]. These works report that their filaments with highest amount of loading show more irregular surfaces and are not suitable for printing. To demonstrate the printability of the fabricated magnetic composite filament in this work, several structures with different printing parameters and precision were 3D-printed on a commercial printer with a conventional nozzle of 0.8 mm in diameter using the nominal 12 vol.% magnetic composite filament as an example. Their photos are presented in Figure 8. Printing temperatures were lowered from the conventional 215˚C to 170 ˚C, which affects the resolution of printing the 3D cubes (5 x 5 x 5 mm) as shown in in the top panel of Figure 8: a well-resolved layer-by-layer construction of the cube is observed towards the right with lowered temperatures. The inclusion of the metallic particles increases the heat transfer of the composite filament, making it much more fluid than the filler-free PLA filament for the same printing temperature. Thus, the resolution of printed structures with the composite filament could be improved by lowering the printing temperature from 215 ˚C (the usual for that PLA) down to 170 ˚C. The temperature for printing the composite, although it is considerably lower than the one for PLA, does not cause nozzle clogging since the melting state and viscosity of the composite were adequate for printing. With the optimized printing temperature, more various structures (hollow cube 20 x 20 x 10 mm and hollow cylinder φ_{outer} 20 x 10 mm) with higher printing density of 100% infill were printed (shown in the bottom panel of Figure 8). Furthermore, structures of varying layer height can be properly controlled by the 3D printer and custom-made magnetic composite filament as seen on the right of the bottom panel of Figure 8 (φ_{outer} 20 x 10 mm).

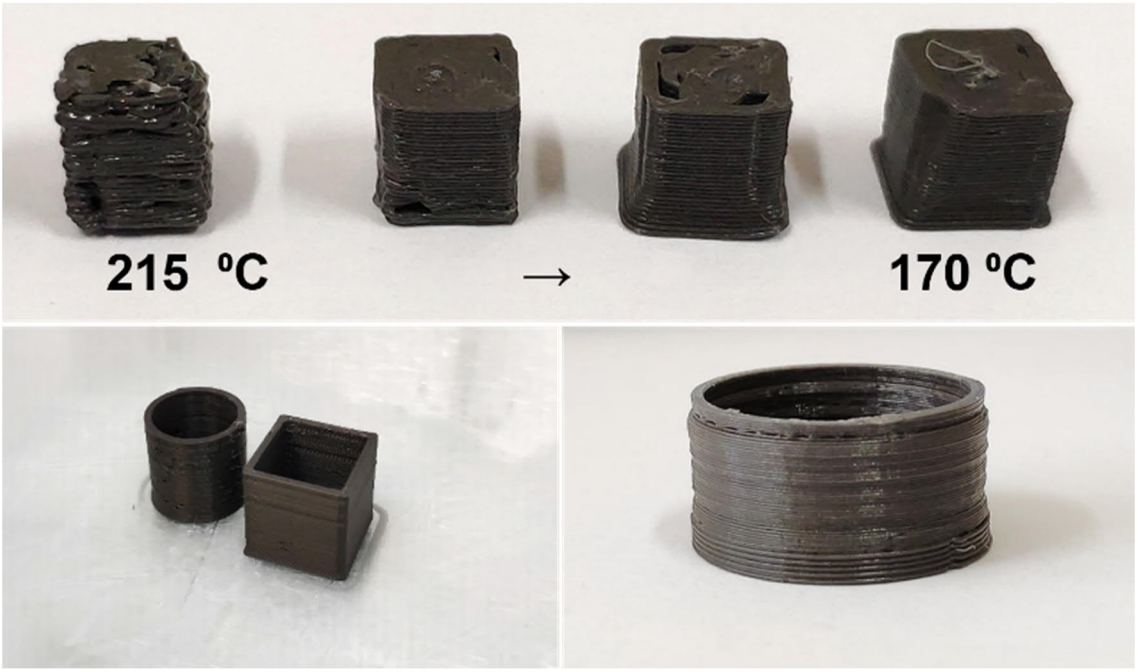

Figure 8. Demonstration of 3D printing of the fabricated magnetic composite filament.

5 Conclusions

A new procedure for the preparation of composite filaments for material extrusion additive manufacturing at the laboratory scale has been presented. It allows obtaining uniformly distributed magnetic particles in the polymer matrix without the need of previous kneading of the feedstock, as evidenced by X-ray tomography and scanning electron microscopy images. The procedure consists in using custom-design capsules filled with powders as the feedstock for filament extrusion. In this way, the feedstock reaches the melting area of the extruder with the appropriate concentration of fillers. At the laboratory scale, capsules can be printed to facilitate the study of different constituents of the composite, having full control over the polymer and the fillers, therefore enabling research on the properties of the composites and printed parts, without being restricted to commercial filaments or using sophisticated instrumentation. This technique can also be transferred to larger scale production when capsules could be fabricated with massive production techniques, such as vacuum forming, and automatically filled with the desired material.

The filament fabricated with the new method has been exhaustively characterized by using different advanced measurement techniques that complement and reinforce each other. The morphological characteristics have been studied by X-ray tomography and SEM, obtaining results that indicate a uniform distribution of particles within the polymer matrix without

agglomerations. Among other useful values, X-ray tomography allows to obtain the composition in volume % of fillers, which is in good agreement with the nominal composition. The functional magnetic properties of composite filaments have been analyzed through magnetization measurements and Kerr microscopy, giving results in good agreement with the characteristics of the fillers. The saturation magnetizations of filament samples also allow to obtain the fraction of magnetic fillers when comparing with the experimental saturation magnetization of the magnetic powder, giving results in good agreement with X-ray tomography and nominal compositions. Kerr microscopy also provides details about a good particle distribution as no evidences of stray-field interaction between the particles were concluded.

Therefore, the combination of the different characterization techniques that have been used provides a reliable validation of the proposed manufacturing method, as well as a complete description of the properties that should be known for the applicability of this type of composite filaments for printing functional parts.

6 Acknowledgements

This work was supported by AEI/FEDER-UE (project MAT-2016-77265-R), FEDER Operating Program 2014-2020 and Consejería de Economía y Conocimiento of the Regional Government of Andalucia (US-1260179), and Plan Andaluz de Investigación, Desarrollo e Innovación (P18-RT-746). The authors extend special thanks to Soléne Valton (RX Solutions) for her assistance in acquiring the tomography data, Stefan Pofahl and Katja Berger (both IFW) for preparing the sample for Kerr microscopy, and Pablo Carmona for his assistance in preparing the samples for VSM.

7 Data availability

The data that support the findings of this study are available from the corresponding author on reasonable request. Videos including 3D reconstruction of the composite filament are available in the supplementary information.

8 References

1 W. Zhong, F. Li, Z. Zhang, L. Song and Z. Li, *Mater. Sci. Eng. A*, 2001, 301, 125–130.
2 L. M. Bollig, M. V. Patton, G. S. Mowry and B. B. Nelson-Cheeseman, *IEEE Trans. Magn.*, 2017, 53, 1–6.
3 B. Khatri, K. Lappe, D. Noetzel, K. Pursche and T. Hanemann, *Materials (Basel).*, 2018, 11, 189.
4 K. von Petersdorff-Campen, Y. Hauswirth, J. Carpenter, A. Hagmann, S. Boës, M. Schmid Daners, D. Penner and M. Meboldt, *Appl. Sci.*, 2018, 8, 1275.
5 L. M. Bollig, P. J. Hilpisch, G. S. Mowry and B. B. Nelson-Cheeseman, *J. Magn. Magn. Mater.*, 2017, 442, 97–101.
6 M. V. Patton, P. Ryan, T. Calascione, N. Fischer, A. Morgenstern, N. Stenger and B. B. Nelson-

Cheeseman, *Addit. Manuf.*, 2019, 27, 482–488.
7 J. C. Tan and H. Y. Low, *Addit. Manuf.*, 2018, 23, 294–302.
8 S. Waheed, J. M. Cabot, P. Smejkal, S. Farajikhah, S. Sayyar, P. C. Innis, S. Beirne, G. Barnsley, T. W. Lewis, M. C. Breadmore and B. Paull, *ACS Appl. Mater. Interfaces*, 2019, 11, 4353–4363.
9 M. Nikzad, S. H. Masood and I. Sbarski, *Mater. Des.*, 2011, 32, 3448–3456.
10 S. W. Kwok, K. H. H. Goh, Z. D. Tan, S. T. M. Tan, W. W. Tjiu, J. Y. Soh, Z. J. G. Ng, Y. Z. Chan, H. K. Hui and K. E. J. Goh, *Appl. Mater. Today*, 2017, 9, 167–175.
11 S. Dul, L. Fambri and A. Pegoretti, *Nanomaterials*, 2018, 8, 49.
12 A. P. Taylor, C. Velez Cuervo, D. P. Arnold and L. F. Velasquez-Garcia, *J. Microelectromechanical Syst.*, 2019, 28, 481–493.
13 S. Fafenrot, N. Grimmelsmann, M. Wortmann and A. Ehrmann, *Materials (Basel).*, 2017, 10, 1199.
14 S. Banerjee and A. K. Tyagi, *Functional Materials*, Elsevier, 2012.
15 K. J. Miller, K. N. Collier, H. B. Soll-Morris, R. Swaminathan and M. E. McHenry, *J. Appl. Phys.*, 2009, 105, 1–4.
16 E. Çanti, M. Aydın and F. Yıldırım, *J. Polytech.*, 2018, 21, 397–402.
17 B. Khatri, K. Lappe, M. Habedank, T. Mueller, C. Megnin and T. Hanemann, *Polymers (Basel).*, 2018, 10, 666.
18 J. Gonzalez-Gutierrez, S. Cano, S. Schuschnigg, C. Kukla, J. Sapkota and C. Holzer, *Materials (Basel).*, 2018, 11, 840.
19 P. Parsons, Z. Larimore, F. Muhammed and M. Mirotznik, *Addit. Manuf.*, 2019, 30, 100888.
20 E. M. Palmero, D. Casaleiz, N. A. Jimenez, J. Rial, J. De Vicente, A. Nieto, R. Altimira and A. Bollero, *IEEE Trans. Magn.*, 2019, 55, 2101004.
21 E. M. Palmero, D. Casaleiz, J. de Vicente, J. Hernández-Vicen, S. López-Vidal, E. Ramiro and A. Bollero, *Compos. Part A Appl. Sci. Manuf.*, 2019, 124, 105497.
22 I. Antoniac, D. Popescu, A. Zapciu, A. Antoniac, F. Miculescu and H. Moldovan, *Materials (Basel).*, 2019, 12, 1–13.
23 D. Legland, I. Arganda-Carreras and P. Andrey, *Bioinformatics*, 2016, 32, 3532–3534.
24 J. Schindelin, I. Arganda-Carreras, E. Frise, V. Kaynig, M. Longair, T. Pietzsch, S. Preibisch, C. Rueden, S. Saalfeld, B. Schmid, J.-Y. Tinevez, D. J. White, V. Hartenstein, K. Eliceiri, P. Tomancak and A. Cardona, *Nat. Methods*, 2012, 9, 676–82.
25 C. T. Rueden, J. Schindelin, M. C. Hiner, B. E. DeZonia, A. E. Walter, E. T. Arena and K. W. Eliceiri, *BMC Bioinformatics*, 2017, 18, 1–26.
26 R. Schäfer, in *Handbook of Magnetism and Advanced Magnetic Materials*, John Wiley & Sons, Ltd, Chichester, UK, 2007.
27 V. Hoffmann, R. Schäfer, E. Appel, A. Hubert and H. Soffel, *J. Magn. Magn. Mater.*, 1987, 71, 90–94.
28 A. V. Shenoy, *Rheology of Filled Polymer Systems*, Springer Netherlands, Dordrecht, 1999.
29 J. Jancar and A. T. Dibenedetto, *J. Mater. Sci.*, 1995, 30, 1601–1608.
30 A. Dufresne, *Cellulose-Based Composites and Nanocomposites*, Elsevier, 2013.
31 F. L. S. Geurts, A. M. van Herk and A. L. German, *J. Microencapsul.*, 2001, 18, 533–543.
32 M. Spoerk, F. Arbeiter, I. Raguž, G. Weingrill, T. Fischinger, G. Traxler, S. Schuschnigg, L. Cardon and C. Holzer, *Macromol. Mater. Eng.*, 2018, 303, 1800179.
33 I. V. Soldatov and R. Schäfer, *Rev. Sci. Instrum.*, 2017, 88, 073701.
34 A. Hubert and R. Schäfer, *Magnetic Domains*, Springer Berlin Heidelberg, Berlin, Heidelberg, 1998.